JACS
JOURNAL OF THE AMERICAN CHEMICAL SOCIETY
Article
pubs.acs.org/JACS

Diffusion-Controlled Detection of Trinitrotoluene: Interior Nanoporous Structure and Low Highest Occupied Molecular Orbital Level of Building Blocks Enhance Selectivity and Sensitivity

Yanke Che,[†,‡] Dustin E. Gross,[§,‡] Helin Huang,[†] Dongjiang Yang,[∥] Xiaomei Yang,[†] Emre Discekici,[§] Zheng Xue,[§] Huijun Zhao,[∥] Jeffrey S. Moore,*[,§] and Ling Zang*[,†]

[†]Department of Materials Science and Engineering, The University of Utah, Salt Lake City, Utah 84108, United States
[§]Departments of Chemistry, University of Illinois at Urbana−Champaign, Urbana, Illinois 61801, United States
[∥]Environmental Futures Centre, Griffith School of Environment, Griffith University, Queensland 4222, Australia

Supporting Information

ABSTRACT: Development of simple, cost-effective, and sensitive fluorescence-based sensors for explosives implies broad applications in homeland security, military operations, and environmental and industrial safety control. However, the reported fluorescence sensory materials (e.g., polymers) usually respond to a class of analytes (e.g., nitroaromatics), rather than a single specific target. Hence, the selective detection of trace amounts of trinitrotoluene (TNT) still remains a big challenge for fluorescence-based sensors.

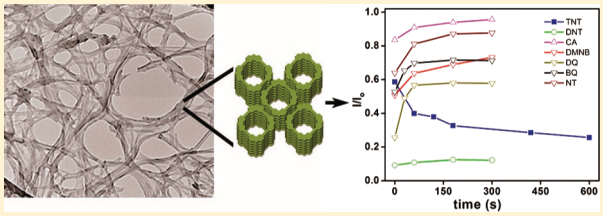

Here we report the selective detection of TNT vapor using the nanoporous fibers fabricated by self-assembly of carbazole-based macrocyclic molecules. The nanoporosity allows for time-dependent diffusion of TNT molecules inside the material, resulting in further fluorescence quenching of the material after removal from the TNT vapor source. Under the same testing conditions, other common nitroaromatic explosives and oxidizing reagents did not demonstrate this postexposure fluorescence quenching; rather, a recovery of fluorescence was observed. The postexposure fluorescence quenching as well as the sensitivity is further enhanced by lowering the highest occupied molecular orbital (HOMO) level of the nanofiber building blocks. This in turn reduces the affinity for oxygen, thus allocating more interaction sites for TNT. Our results present a simple and novel way to achieve detection selectivity for TNT by creating nanoporosity and tuning molecular electronic structure, which when combined may be applied to other fluorescence sensor materials for selective detection of vapor analytes.

INTRODUCTION

Trace explosive detection has drawn intense attention due to the increasing concern in homeland security, military operation safety, and environmental and industrial safety control.[1−9] Among the current detection technologies, fluorescence-based sensors are simple, cost-effective, and highly sensitive detection modalities.[1,3,8] However, the fluorescence sensory materials (e.g., polymers) reported thus far usually respond to a class of analytes (e.g., nitroaromatics), rather than a single specific target.[1,9] For example, most of the sensory materials developed for the detection of TNT are also sensitive to other nitro-organic compounds and many other oxidizing reagents such as quinones.[2] Although field security monitoring of a class of explosives or threats can be beneficial, development of a fluorescence-based sensor system with selectivity for a specific target is critical for chemical identification and background analysis of terrorism activities. Therefore, the selective detection of trinitrotoluene (TNT) in conjunction with high sensitivity is highly desirable, though it still remains a big challenge for optical sensors, which usually have indiscriminant interfacial binding to analytes.

Recently, a metal−organic framework (MOF) has been reported to allow amines of different sizes to diffuse into its channels with time-dependent quenching behavior,[10] thus enabling identification of the type of amine. This inspired us to explore the selective detection of TNT using porous nanofibers fabricated from p-type organic semiconductor molecules. Given that TNT has very low volatility along with strong binding to sensing materials via electron donor−acceptor and $\pi-\pi$ interactions, it is expected that the diffusion of TNT within porous nanofibers should be significantly slower than that of other explosives or oxidizing reagents. This may generate different fluorescence quenching behaviors, thereby enabling distinction of TNT from other oxidizing reagents. In the present work, two types of porous nanofiber materials were employed for studying the selective detection of TNT through fluorescence-based quenching. The first is composed of "piled nanofibers", which form a porous material upon entangled piling of the solid nanofibers. The second is "piled nanoporous nanofibers", which are doubly porous by entangled piling of inherently porous nanofibers (Figure 1). Furthermore, macrocyclic building blocks with a lower highest occupied molecular orbital (HOMO) level, which can reduce the interaction with

Received: January 11, 2012
Published: February 16, 2012

   dx.doi.org/10.1021/ja300306e | J. Am. Chem. Soc. 2012, 134, 4978−4982

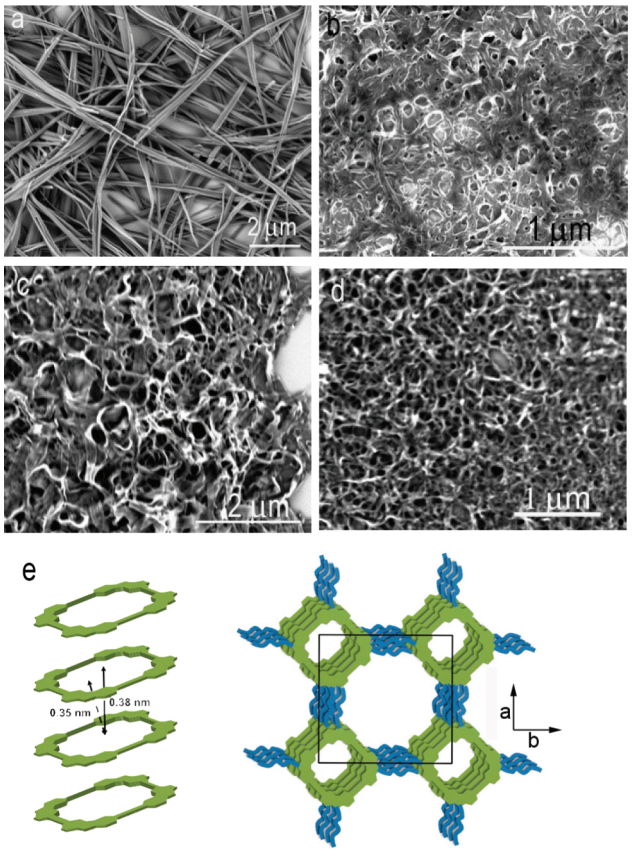

Figure 1. SEM image of nanoporous nanofibers fabricated from (a) **1** and (b) **2** and porous nanofibers films from (c) **4** and (d) **5**. (e) Modeling of tubular or nanoporous packing of **1** and the rectangular lattice.

oxygen, are also investigated for improvement of sensing properties.

RESULTS AND DISCUSSION

The carbazole-based tetracycles (TC) **1**–**3** (Scheme 1) were synthesized following our previous method,[11,12] and the oligomers **4** and **5** were synthesized by standard protocols (see Supporting Information). All nanofibers were fabricated via a new self-assembly process under low-temperature conditions (see Supporting Information for details), allowing for slow Oswald ripening in a binary solvent system. With this method, long nanofibril structures were formed as revealed by scanning electron microscopy (SEM) imaging (Figure 1). Porosity can be achieved by piling (spin-casting) the nanofibers, which were prefabricated in solution (Figure 1a–d). Among these, well-defined larger nanofibers were fabricated from **1**, due to its shorter alkyl side chains (Figure 1a). The large size and straight morphology of the nanofibers make the piling with large pores, or interstices, in the range of micrometers. Although transmission electron microscopy (TEM) imaging (Figure S1, Supporting Information) does not reveal the nanoporous structures of nanofibers fabricated from **1** or **2** (in a similar manner as reported for carbon nanotubes), the long-range tubular stacking is evidenced by X-ray diffraction (XRD) measurements (Figure S2, Supporting Information). XRD of nanofibers of **1** displayed pronounced diffraction peaks (Figure S2a, Supporting Information), which can be assigned to a two-dimensional (2D) rectangular lattice with lattice parameters a and b of 2.24 nm. The d-spacing values of 0.38 nm at $2\theta = 23.4°$ and 0.35 nm at $2\theta = 25.5°$ are assignable to the center-to-center distance and π–π stacking distance of tilted macrocycles, respectively, suggesting that molecules of **1** most likely adopt a cofacial orientation with a tilting angle of 23° (i.e., small lateral offset of 0.15 nm) relative to the long axis of the resulting column (Figure 1e). This slipped stacking of **1** is also consistent with the red-shifted absorption and emission as measured over the nanofibers, in comparison to that of individual molecules dissolved in solutions (Figure S3, Supporting Information), indicative of J-aggregate formation.[13] The nanoporous structure as dominated by the tubular stacking was confirmed by the greater intensity observed at higher-order XRD peaks (22, 40), which are typically characteristic of porous tubular nanostructures.[14,15] The hydrophobic interaction between alkyl chains is also supported by the observed diffraction peak with a d-spacing of ca. 0.43 nm, typical of ordered paraffinic side chains.[16] Similarly, the diffraction pattern of **2** nanofibers can be indexed to a 2D rectangular lattice but with larger lattice parameters of a and b of 2.48 nm, consistent with longer side chains in **2**, and higher intensity of the higher-order diffraction peaks (22, 40) indicates the formation of long-range order of the porous tubular nanostructure (Figure S2b, Supporting Information). Carbazole-based oligomer **4**, lacking a molecular cavity, adopts lamellar stacking into solid nanofibers, as evidenced by its XRD data (Figure S4, Supporting Information), where the peaks can be indexed to higher-order diffraction from (002) to (005). Similar intermolecular stacking is expected for the nanofibers of **5**, given the similarity of absorption and emission spectral changes of **5** to those of **4** (Figure S5, Supporting Information). The above observations allow us to conclude that oligomer molecules can form solid nanofibers and subsequently form exterior porous films upon piling, while tetracycle molecules can form nanoporous nanofibers via tubular stacking that can also possess exterior pores from the piling.

Upon exposure to oxidizing reagent vapors such as those listed in Scheme 2, the emission of nanoporous nanofibers was quenched. One such example is shown in Figure 2a, where the fluorescence spectra of nanofibers of **1** were recorded before and after exposure to the saturated vapor of TNT (ca. 5 ppb) for 1 min, indicating 18% fluorescence quenching. Surprisingly, the fluorescence intensity measured over the same nanofibers kept decreasing after removal of the vapor of TNT, that is, reopening the nanofibers to clean air, as shown in Figure 2b. This is in contrast to the cases of exposure to other oxidizing

Scheme 1

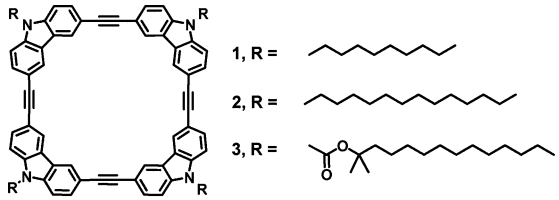

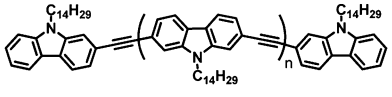

4, n=1; 5, n=3

dx.doi.org/10.1021/ja300306e | J. Am. Chem. Soc. 2012, 134, 4978–4982

Scheme 2

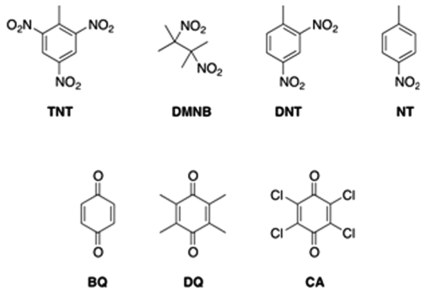

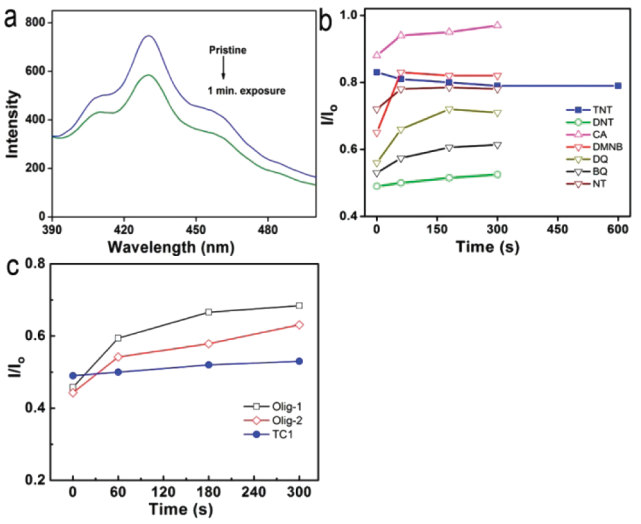

Figure 2. (a) Fluorescence spectra recorded over the nanoporous nanofibers of **1** recorded before and after exposure to the saturated TNT vapor (5 ppb) for 1 min. (b) Postexposure fluorescence intensity change (I/I_0) measured over the same nanofibers of **1** as a function of time after reopening to clean air. The values at time zero represent the fluorescence intensity measured after 20 s of exposure to the saturated vapor of various oxidizing reagents and 1 min of exposure to the saturated vapor of TNT. (c) Postexposure fluorescence intensity change (I/I_0) measured over three different nanofibers as function of time after reopening to clean air. The values at time zero represent the fluorescence intensity measured after 20 s of exposure to the saturated vapor of DNT (100 ppb). Error bar: ±6%.

reagent vapors, for which no such postexposure fluorescence quenching was observed; rather the fluorescence emission was recovered to certain extents. The emission recovery is apparently due to the release of volatile reagents from the nanofibril pores. Noticeably, the smallest extent of recovery was found for dinitrotoluene (DNT), likely due to its similar size and chemical properties as TNT. The postexposure continuous quenching observed with TNT implies some diffusion-controlled process within the porous structure, which may be constituted by the interior tubular structure of the nanofiber or the interfibril interstices caused by tight entangled piling of nanofibers. In addition, considering the extended exciton migration typically expected for columnar aromatics and the fibril materials,[17−22] sparse distribution of a quencher upon slow diffusion within the range of exciton migration distance also helps maximize the fluorescence quenching efficiency. The same experiments were also performed over the nanoporous nanofibers fabricated from **2** and demonstrated quite similar behavior as observed for the nanoporous nanofibers of **1**, as shown in Figure 2a,b. The distinctive postexposure fluorescence quenching observed for TNT provides a new way to selectively detect TNT from other nitro-based explosives or oxidizing reagents. The observations herein, primarily relying on dynamic characterization, may open an alternative way to approach detection selectivity, where the diffusion dynamics is determined by a combination of several characteristics of the guest molecules interacting with the porous nanofibers, including size, volatility, and interfacial binding.

To explore whether the porosity constituted by the interfibril piling plays a critical role in determining the slow diffusion dynamics of TNT as observed above, the same quenching measurements as shown in Figure 2a,b were performed over the solid nanofibers fabricated from oligomers **4** and **5**. These solid nanofibers demonstrated very low fluorescence quenching upon exposure to saturated vapor of TNT; that is, only <5% quenching was observed after 1 min of exposure. The low quenching efficiency is likely due to poor accumulation of the low vapor of TNT. Due to this low quenching, DNT was used instead to study the postexposure fluorescence changing as performed above over the interior porous nanofibers of **1** and **2**. As shown in Figure 2c, ca. 55% fluorescence quenching was observed for nanofibers of **4** and **5** upon exposure to the saturated vapor of DNT for 20 s. However, the fluorescence was considerably recovered upon reopening to clean air. This is in contrast to the observation over the nanoporous nanofibers of **1**, for which the fluorescence was recovered significantly more slowly and only to a minimal extent (Figure 2c). These results suggest that exterior porosity constituted by the solid nanofibers can hardly afford the slow diffusion of guest molecules to enable postexposure fluorescence quenching. This is likely due to the near micropore size that causes easy desorption of analytes upon re-exposure (equilibrated) to clean air, thus leading to recovery of fluorescence.

Although the new nanoporous nanofibers of **1** and **2** have proven the feasibility of selective detection of TNT based on the postexposure fluorescence quenching, the postexposure fluorescence quenching is modest and the sensor sensitivity is relatively low compared to other fluorescence sensor systems.[1,3] This is likely due to the competitive adsorption caused by the ubiquitous oxygen present inside the materials, where oxygen is believed to bind to the same site (i.e., the carbazole moiety) on the internal surface of nanofiber. The strong binding interaction between oxygen and the nanoporous nanofibers of **1** and **2** was implied by the enhanced photocurrent as obtained in the presence of oxygen (Figure S6, Supporting Information). To further increase the fluorescence sensing efficiency, it is essential to reduce the oxygen adsorption so as to accommodate more binding sites for the gas analytes. To approach this, we changed the building block to **3**, which possesses the same backbone as **1** and **2** and can be fabricated into similar tubular nanofibers (Figure S7, Supporting Information). Because of the introduction of a carboxyl group into the side-chain linker, the HOMO energy level of the molecule is significantly lowered down to −5.6 eV, compared to that of **1** and **2** (both at −4.9 eV).[8] Decreasing the HOMO level of organic molecules represents a general strategy to improve their stability against oxygen.[23] It is thus expected that the nanoporous nanofibers of **3** possess much weaker interaction with oxygen, thereby facilitating the intake of TNT. The weak interaction with oxygen of **3** was consistent with the negligible photocurrent as measured over the nanofibers of **3** in the presence of oxygen.[24] We previously reported the efficient fluorescence quenching of a spin-cast

dx.doi.org/10.1021/ja300306e | J. Am. Chem. Soc. 2012, 134, 4978−4982

nanofibril film of **3** upon exposure to the vapor of TNT and DNT.[8] However, such film was found to exhibit similar fluorescence quenching behavior for various kinds of oxidizing reagents; that is, there was a lack of selectivity for a single specific explosive target, probably due to no interior pores morphology formed by this processing. Here, we fabricated molecules of **3** into nanoporous nanofibers using the same self-assembly method as employed for **1** and **2**. The greater intensity observed at higher-order XRD peaks (22, 40) is indicative of the tubular porous structure of the nanofiber fabricated from **3** (Figure S8, Supporting Information). Similarly to the nanofibers of **1** and **2**, a two-dimensional rectangular lattice with lattice parameters *a* and *b* of 2.52 nm can be deduced from the XRD data, while the formation of J-aggregation can be indicated by the optical measurements (Figure S9, Supporting Information).

As shown in Figure 3a, the fluorescence recorded from the nanofibers made from **3** was effectively quenched by 40% upon exposure to the saturated vapor of TNT for only 10 s. More strikingly, significant postexposure fluorescence quenching was observed as shown in Figure 3b,c, where the fluorescence continued to decrease by another 35% within 10 min after reopening to clean air. In addition to the enhanced selectivity toward TNT as enabled by the postexposure fluorescence quenching, the new nanofibers of **3** also demonstrated enhanced sensitivity for vapor detection of this explosive; that is, 75% fluorescence quenching was achieved upon only 10 s of initial vapor exposure. In comparison, only 20% quenching after 1 min of exposure was observed for nanofibers of **1** that possess similar interior porosity as revealed by the XRD measurements. When tested for DNT, as high as 90% fluorescence quenching was attained for the similar nanofibers of **3** within 10 s of exposure, whereas only 50% fluorescence quenching was achieved for the nanofibers of **1** upon 20 s of exposure. Clearly, a reduced interaction between the nanoporous nanofibers and oxygen can effectively improve the intake of TNT within the porosity, thereby enhancing both sensing selectivity and sensitivity.

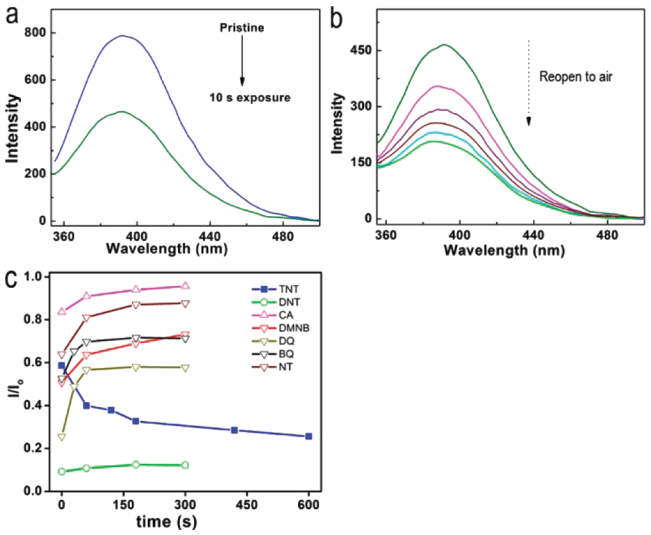

Figure 3. Fluorescence quenching measured over nanoporous nanofibers from **3**. (a) Fluorescence spectra recorded over the nanofibers before and after exposure to saturated TNT vapor (5 ppb) for 10 s. (b) Fluorescence spectra recorded continuously over the same nanofibers at different time intervals after reopening to clean air: 0, 1, 2, 3, 7, and 10 min. (c) Postexposure fluorescence intensity change (I/I_0) measured over the nanofibers as function of time after reopening to clean air. The values at time zero represent the fluorescence intensity measured after 10 s of exposure to the saturated vapor of different oxidizing reagents including TNT. Error bar: ±5%.

To further confirm the strong encapsulation and deep distribution of TNT within the interior pores of nanofibers, nanofibers of **3** after exposure were subsequently immersed in a saturated vapor of hydrazine, which has been proven effective for recovering the fluorescence of conducting polymers and organic nanomaterials after exposure to nitroaromatic explosives.[1,8] Strikingly, the quenched fluorescence of nanoporous nanofibers of **3** remained almost unchanged after immersion in the saturated vapor of hydrazine for 1 min followed by drying in a stream of nitrogen (Figure S10, Supporting Information). In contrast, the fluorescence of the nanofibers made from **4** and **5** was restored to over 90% under the same recovery conditions. Additionally, the *solid* nanofibers fabricated (by previous spin-cast methods[8]) from **3** demonstrated a similar level of fluorescence recovery under the same experimental conditions. These results indicate that the performance and sensing of the organic materials is highly dependent on processing. Additionally, the unrecoverable quenching observed with nanoporous nanofibers reflects a strong, steady-state host–guest interaction between **3** and TNT, which is consistent with the postexposure quenching as observed (Figure 3c).

With the highly efficient encapsulation of vapor analytes proven above for the interior porous nanofibers, we attempted to pursue the lowest detection limit of TNT. Quantitative evaluation of the detection limit was performed at the Naval Research Lab, where a recently built vapor generator provides various levels of vapor pressures for TNT at a range of temperatures. The vapor sensing test was carried out in situ in a home-built optical chamber connected with a photomultiplier tube (PMT) photon detector through an optical fiber. As shown in Figure 4, the interior porous nanofibers made from **3** demonstrated significant emission quenching (ca. 15%) by TNT vapor down to a few tens of parts per trillion (ppt). Upon increasing the vapor pressure of TNT to the range of 2–8 ppb, the quenching efficiency was increased up to ca. 90%. The total response time (about 400 s, defined from the point of

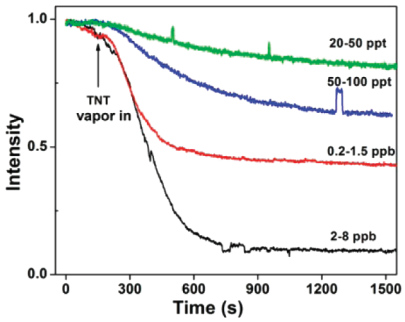

Figure 4. Interior porous nanofibers from **3** demonstrate efficient fluorescence quenching upon exposure to the diluted vapor of TNT: relative fluorescence intensity measured as a function of time of vapor exposure. Tests were performed at four vapor concentration levels: (1, black) 2–8 ppb, (2, red) 0.2–1.5 ppb, (3, blue) 50–100 ppt, and (4, green) 20–50 ppt. The pulsed noise was due to accidental bumping of the table, causing disturbance to the optical fibers. Repeating the experiment three times showed similar results.

dx.doi.org/10.1021/ja300306e | J. Am. Chem. Soc. 2012, 134, 4978–4982

introduction of TNT vapor to the turning point of quenching saturation) represents the slow vapor saturation process in the relatively large optical chamber, rather than the sensing response of the materials. To the best of our knowledge, the obtained detection limit of a few tens of parts per trillion places the nanoporous fibers among the most sensitive materials tested under the same conditions (i.e., without elaborate optimization and integration into a instrument).[25] Interestingly, no fluorescence recovery was observed after stopping the explosive exposure and reopening to clean air, consistent with a strong encapsulation of explosives.

CONCLUSION

In conclusion, we demonstrate that nanoporous nanofibers fabricated from carbazole-based tetracycles allow for slow diffusion and strong encapsulation of TNT molecules within the nanopores, thus resulting in postexposure fluorescence quenching behavior, which enables selective detection of TNT among other common nitroaromatic explosives and oxidizing reagents. In contrast, the porosity caused by entangled piling of nanofibers exhibits no postexposure fluorescence quenching. When carbazole-based tetracycles with a decreased HOMO energy level, which can reduce the interaction with oxygen and thus enhance the adsorption of TNT, were chosen, the postexposure fluorescence quenching observed over the interior porous nanofibers became more prominent, along with an enhanced sensitivity. A combination of nanoporosity and tunable HOMO energy level provides a feasible way to achieve selective detection of TNT at sufficiently low detection limits. Such a strategy may be extended to other fluorescence-based sensing materials to approach selective detection of a specific analyte.

ASSOCIATED CONTENT

Supporting Information

Additional text, four schemes, and 10 figures with synthetic details of carbazole-based tetracycles **1**−**3** and oligomers **4** and **5**, optical and XRD characterization of the assembled nanofibers, *I*−*V* curve of interior porous nanofibers from **1**, and TEM images of the interior porous nanofibers. This material is available free of charge via the Internet at http://pubs.acs.org.

AUTHOR INFORMATION

Corresponding Author

jsmoore@illinois.edu; lzang@eng.utah.edu

Author Contributions

‡These authors contributed equally.

Notes

The authors declare no competing financial interest.

ACKNOWLEDGMENTS

This work was supported by NSF (CAREER CHE 0641353, CBET 730667), DHS (2009-ST-108-LR0005), and USTAR Program. We thank Greg Collins and Susan L. Rose-Pehrsson at Naval Research Laboratory for the measurements with diluted TNT vapors, which is part of the work by the Trace Explosives Test Bed Team in the Chemistry Division (Code 6100).

REFERENCES

(1) Thomas, S. W.; Joly, G. D.; Swager, T. M. *Chem. Rev.* **2007**, *107*, 1339.
(2) Yang, J.-S.; Swager, T. M. *J. Am. Chem. Soc.* **1998**, *120*, 11864.
(3) Lan, A.; Li, K.; Wu, H.; Olson, D. H.; Emge, T. J.; Ki, W.; Hong, M.; Li, J. *Angew. Chem., Int. Ed.* **2009**, *48*, 2334.
(4) Toal, S. J.; Trogler, W. C. *J. Mater. Chem.* **2006**, *16*, 2871.
(5) Engel, Y.; Elnathan, R.; Pevzner, A.; Davidi, G.; Flaxer, E.; Patolsky, F. *Angew. Chem., Int. Ed.* **2010**, *49*, 6830.
(6) Lin, H.; Suslick, K. S. *J. Am. Chem. Soc.* **2010**, *132*, 15519.
(7) Diaz Aguilar, A.; Forzani, E. S.; Leright, M.; Tsow, F.; Cagan, A.; Iglesias, R. A.; Nagahara, L. A.; Amlani, I.; Tsui, R.; Tao, N. J. *Nano Lett.* **2010**, *10*, 380.
(8) Naddo, T.; Che, Y.; Zhang, W.; Balakrishnan, K.; Yang, X.; Yen, M.; Zhao, J.; Moore, J. S.; Zang, L. *J. Am. Chem. Soc.* **2007**, *129*, 6978.
(9) Germain, M. E.; Knapp, M. J. *Chem. Soc. Rev.* **2009**, *38*, 2543.
(10) Wang, C.; Lin, W. *J. Am. Chem. Soc.* **2011**, *133*, 4232.
(11) Finke, A. D.; Gross, D. E.; Han, A.; Moore, J. S. *J. Am. Chem. Soc.* **2011**, *133*, 14063.
(12) Zhang, W.; Moore, J. S. *Angew. Chem., Int. Ed.* **2006**, *45*, 4416.
(13) Würthner, F.; Kaiser, T. E.; Saha-Möller, C. R. *Angew. Chem., Int. Ed.* **2011**, *50*, 3376.
(14) Peterca, M.; Percec, V.; Dulcey, A. E.; Nummelin, S.; Korey, S.; Ilies, M.; Heiney, P. A. *J. Am. Chem. Soc.* **2006**, *128*, 6713.
(15) Percec, V.; Peterca, M.; Dulcey, A. E.; Imam, M. R.; Hudson, S. D.; Nummelin, S.; Adelman, P.; Heiney, P. A. *J. Am. Chem. Soc.* **2008**, *130*, 13079.
(16) Hosono, N.; Kajitani, T.; Fukushima, T.; Ito, K.; Sasaki, S.; Takata, M.; Aida, T. *Science* **2010**, *330*, 808.
(17) Zang, L.; Che, Y.; Moore, J. S. *Acc. Chem. Res.* **2008**, *41*, 1596.
(18) Lin, H.; Camacho, R.; Tian, Y.; Kaiser, T. E.; Wurthner, F.; Scheblykin, I. G. *Nano Lett.* **2010**, *10*, 620.
(19) Zhao, Y. S.; Fu, H.; Peng, A.; Ma, Y.; Liao, Q.; Yao, J. *Acc. Chem. Res.* **2010**, *43*, 409.
(20) Chaudhuri, D.; Li, D.; Che, Y.; Shafran, E.; Gerton, J. M.; Zang, L.; Lupton, J. M. *Nano Lett.* **2011**, *11*, 488.
(21) Adams, D. M.; Kerimo, J.; Olson, E. J. C.; Zaban, A.; Gregg, B. A.; Barbara, P. F. *J. Am. Chem. Soc.* **1997**, *119*, 10608.
(22) Hughes, R. E.; Hart, S. P.; Smith, D. A.; Movaghar, B.; Bushby, R. J.; Boden, N. *J. Phys. Chem. B* **2002**, *106*, 6638.
(23) Usta, H.; Facchetti, A.; Marks, T. J. *Acc. Chem. Res.* **2011**, *44*, 501.
(24) Che, Y.; Yang, X.; Zhang, Z.; Zuo, J.; Moore, J. S.; Zang, L. *Chem. Commun.* **2010**, *46*, 4127.
(25) Cumming, C. J.; Aker, C.; Fisher, M.; Fok, M.; la Grone, M. J.; Reust, D.; Rockley, M. G.; Swager, T. M.; Towers, E.; Williams, V. *IEEE Trans. Geosci. Remote Sens.* **2001**, *39*, 1119.